



Teleportation of Nonclassical Wave Packets of Light

Noriyuki Lee, et al. Science **332**, 330 (2011); DOI: 10.1126/science.1201034

This copy is for your personal, non-commercial use only.

If you wish to distribute this article to others, you can order high-quality copies for your colleagues, clients, or customers by clicking here.

Permission to republish or repurpose articles or portions of articles can be obtained by following the guidelines here.

The following resources related to this article are available online at www.sciencemag.org (this infomation is current as of April 14, 2011):

Updated information and services, including high-resolution figures, can be found in the online version of this article at:

http://www.sciencemag.org/content/332/6027/330.full.html

Supporting Online Material can be found at:

http://www.sciencemag.org/content/suppl/2011/04/13/332.6027.330.DC1.html

This article **cites 23 articles**, 2 of which can be accessed free: http://www.sciencemag.org/content/332/6027/330.full.html#ref-list-1

This article has been **cited by** 1 articles hosted by HighWire Press; see: http://www.sciencemag.org/content/332/6027/330.full.html#related-urls

This article appears in the following **subject collections:** Physics

http://www.sciencemag.org/cgi/collection/physics

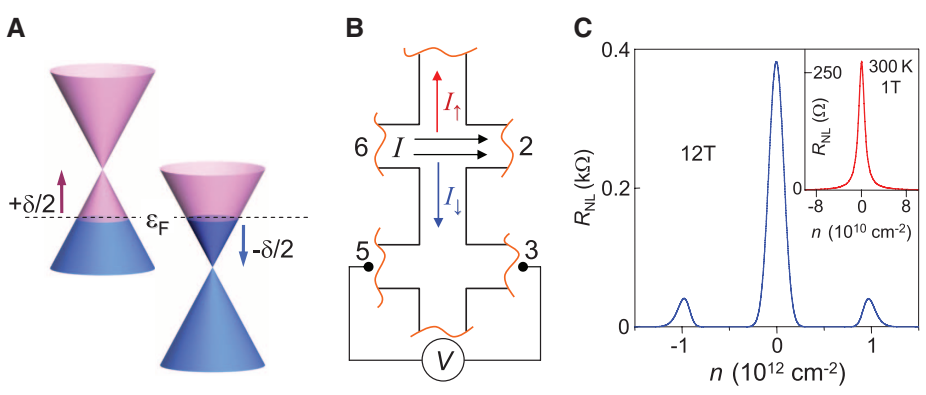


Fig. 3. SHE in graphene and nonlocal transport mediated by spin diffusion. (A) Zeeman splitting at charge neutrality produces two pockets filled with electrons and holes having opposite spin. (B) In the presence of the Lorentz force, I gives rise to transverse spin currents I_{\uparrow} and I_{\downarrow} . Because the force has opposite signs for electrons and holes, the net charge current is zero, whereas the net spin current is nonzero. The resulting imbalance in the up/down spin distribution can reach remote regions and generate a voltage drop V. (C) $R_{\rm NL}$ predicted in our model for the QHE regime (main panel) and the quasiclassical regime (inset). The best-fit parameters $n_0 = 4 \times 10^9$ cm⁻² and Landau level broadening $\Gamma = 200$ K are typical for GBN and GSiO devices, respectively. $R_{\rm NL}$ grows with decreasing n_0 and Γ (17), which is consistent with much larger R_{NL} measured in our GBN devices.

edge-state transport mechanisms, we believe that the spin/valley Hall effect is the only remaining explanation for our findings.

The profound nonlocality described here is an essential attribute of electron transport in graphene. The nonlocality is consistent with neutral currents generated by the SHE at high T and, possibly, by the valley Hall effect at liquid-helium T. Nonlocal transport, being directly sensitive to neutral degrees of freedom, provides valuable information that is inaccessible by conventional electrical measurements.

References and Notes

- 1. A. K. Geim, K. S. Novoselov, Nat. Mater. 6, 183
- 2. A. H. Castro Neto, F. Guinea, N. M. R. Peres, K. S. Novoselov, A. K. Geim, Rev. Mod. Phys. 81, 109
- 3. H. B. Heersche, P. Jarillo-Herrero, J. B. Oostinga, L. M. Vandersypen, A. F. Morpurgo, Nature 446, 56

- 4. A. F. Young, P. Kim, Nat. Phys. 5, 222 (2009).
- 5. J. G. Checkelsky, L. Li, N. P. Ong, Phys. Rev. B 79, 115434 (2009).
- 6. D. A. Abanin et al., Phys. Rev. Lett. 98, 196806 (2007).
- 7. Z. liang, Y. Zhang, H. L. Stormer, P. Kim, Phys. Rev. Lett. 99. 106802 (2007).
- 8. B. E. Feldman, J. Martin, A. Yacoby, Nat. Phys. 5, 889 (2009).
- 9. X. Du. I. Skachko, F. Duerr, A. Luican, E. Y. Andrei, Nature 462, 192 (2009).
- 10. P. L. McEuen et al., Phys. Rev. Lett. 64, 2062 (1990).
- 11. R. J. Haug, Sem. Sci. Tech. 8, 131 (1993).
- 12. Y. Tserkovnyak, S. Brataas, G. E. W. Bauer, B. I. Halperin, Rev. Mod. Phys. 77, 1375 (2005).
- 13. F. J. Jedema, M. S. Nijboer, A. T. Filip, B. J. van Wees, Phys. Rev. B 67, 085319 (2003).
- 14. S. Washburn, R. A. Webb, Rep. Prog. Phys. 55, 1311 (1992).
- 15. C. R. Dean et al., Nat. Nanotechnol. 5, 722 (2010).
- 16. R. V. Gorbachev et al., Small 7, 465 (2011).
- 17. See supporting material on Science Online.
- 18. L. J. van der Pauw, Philips Tech. Rev. 20, 220 (1958).
- 19. Y. J. Song et al., Nature 467, 185 (2010).
- 20. J. Sinova et al., Phys. Rev. Lett. 92, 126603 (2004).
- 21. Y. K. Kato, R. C. Myers, A. C. Gossard, D. D. Awschalom, Science 306, 1910 (2004).
- 22. J. Wunderlich, B. Kaestner, J. Sinova, T. Jungwirth, Phys. Rev. Lett. 94, 047204 (2005).
- 23. N. Tombros, C. Jozsa, M. Popinciuc, H. T. Jonkman, B. J. van Wees, Nature 448, 571 (2007).
- 24. Supported by the Engineering and Physical Research Council (UK), the Royal Society, U.S. Office of Naval Research, U.S. Air Force Office of Scientific Research, and the Körber Foundation. We thank D. Elias, P. Blake, E. Hill, F. Schedin, S. Anissimova, and I. Grigorieva for their help.

Supporting Online Material

www.sciencemag.org/cgi/content/full/332/6027/328/DC1 SOM Text Figs. S1 to S8

References

26 October 2010; accepted 28 February 2011 10.1126/science.1199595

Teleportation of Nonclassical Wave Packets of Light

Noriyuki Lee,¹ Hugo Benichi,¹ Yuishi Takeno,¹ Shuntaro Takeda,¹ James Webb,² Elanor Huntington, Akira Furusawa 1*

We report on the experimental quantum teleportation of strongly nonclassical wave packets of light. To perform this full quantum operation while preserving and retrieving the fragile nonclassicality of the input state, we have developed a broadband, zero-dispersion teleportation apparatus that works in conjunction with time-resolved state preparation equipment. Our approach brings within experimental reach a whole new set of hybrid protocols involving discrete- and continuous-variable techniques in quantum information processing for optical sciences.

n the early development of quantum information processing (QIP), a communication __protocol called quantum teleportation was discovered (1) that involves the transportation of an unknown arbitrary quantum state $|\psi\rangle$ by means of entanglement and classical information. Ex-

¹Department of Applied Physics, School of Engineering, University of Tokyo, 7-3-1 Hongo, Bunkyo-ku, Tokyo 113-8656, Japan. ²Centre for Quantum Computation and Communication Technology, School of Engineering and Information Technology, University College, University of New South Wales, Canberra, ACT 2600, Australia.

*To whom correspondence should be addressed. E-mail: akiraf@ap.t.u-tokyo.ac.jp

perimental realizations of quantum teleportation (2, 3) and more advanced related operations (4) in the continuous-variable regime have been achieved by linear optics methods, although only for Gaussian states so far. However, at least thirdorder nonlinear operations are necessary for building a universal quantum computer (5)—something that Gaussian operations and Gaussian states alone cannot achieve. Photon subtraction techniques based on discrete-variable technology can provide useful nonlinearities and are used to generate Schrödinger's-cat states and other optical non-Gaussian states (6). Schrödinger's-cat states are of particular interest in this context, as they

have been shown to be a useful resource for faulttolerant QIP (7). It is therefore necessary to extend the continuous-variable technology to the technology used in the world of non-Gaussian states.

We have combined these two sets of technologies, and here we demonstrate such Gaussian operations on nonclassical non-Gaussian states by achieving experimental quantum teleportation of Schrödinger's-cat states of light. Using the photon subtraction protocol, we generate quantum states closely approximating Schrödinger's-cat states in a manner similar to (8-11). To accommodate the required time-resolving photon detection techniques and handle the wave-packet nature of these optical Schrödinger's-cat states, we have developed a hybrid teleporter built with continuous-wave light yet able to directly operate in the time domain. For this purpose we constructed a time-gated source of Einstein-Podolsky-Rosen (EPR) correlations as well as a classical channel with zero phase dispersion (12). We were able to bring all the experimental parameters up to the quantum regime, and we performed successful quantum teleportation in the sense that both our input and output states are strongly nonclassical.

A superposition of the quasi-classical coherent state $|\alpha\rangle$ is one of the consensus definitions of a Schrödinger's-cat state |cat>, typically written $|{\rm cat}\rangle^{\infty}|\alpha\rangle \pm |-\alpha\rangle$. Such optical Schrödinger's-cat states are known to be approximated by multiple photon subtractions from a squeezed vacuum state (δ) . In these protocols, a squeezed vacuum state $\hat{S}(s)|0\rangle$ is weakly tapped via a subtraction channel, where $|0\rangle$ is the vacuum state and $\hat{S}(s)$ is the squeezing operator with squeezing parameter s. When a photon detection event occurs in the subtraction channel, $\hat{S}(s)|0\rangle$ is projected by the quantum action of the photon detector onto a non-Gaussian state, which can be tuned to approximate a Schrödinger's-cat state (8-10). The approximation is not perfect and can be quantified by means of the fidelity figure $F_{\rm cat} = |\langle {\rm cat}|\hat{a}\,\hat{S}(s)|0\rangle|^2$ (13).

To represent the superposition nature of these states, we use the Wigner formalism where for any quantum state $|\phi\rangle$ one associates a quasiprobability distribution W(x, p), where x and p are the phase-space position and momentum parameters. W(x, p) is called the Wigner function and holds information exactly equivalent to $|\phi\rangle$ (14). Although the position \hat{x} and momentum \hat{p} quadrature operators and the vector state $|\phi\rangle$ are abstract objects, W(x, p) is always a definite real-valued function that can be numerically reconstructed if one performs a complete phase-resolved sequence of homodyne measurement $\hat{x}\cos\theta + \hat{p}\sin\theta$, a process called quantum tomography (15, 16). W(x, p)is not a true probability distribution, however, as there exist quantum states whose Wigner functions are not positive. $|\phi\rangle$ is defined to be a strongly nonclassical state when its Wigner function W(x, p)fails to be a positive distribution. Negativity in W(x, p) turns out to be an especially useful description of the nonclassicality of a Schrödinger'scat state $|cat\rangle$; $|\alpha\rangle$ and $|-\alpha\rangle$ induce two "classical" Gaussians in phase space, the superposition of which creates an oscillating interference pattern inducing negativity in W(x, p). In contrast, a statistical mixture of $|\alpha\rangle$ and $|-\alpha\rangle$ would never show such negativity.

In a quantum teleportation process, the input $W_{\rm in}$ and output $W_{\rm out}$ Wigner functions are related by the convolution (denoted \circ)

$$W_{\text{out}} = W_{\text{in}} \circ G_{\exp(-r)}$$
 (1)

where r is the EPR correlation parameter, G_{σ} is a normalized Gaussian of standard deviation σ , and \hbar (Planck's constant divided by 2π) has been set to 1 (17). When finite quantum entanglement r is used, $W_{\rm out}$ will be a thermalized copy of $W_{\rm in}$. Only with infinite r will G_{σ} become a delta function so that $W_{\rm in} = W_{\rm out}$. The quality of quantum teleportation is usually evaluated according to the teleportation fidelity $F_{\rm tele} = \langle \phi^{\rm in} | \hat{\rho}^{\rm out} | \phi^{\rm in} \rangle$, which can be written as $F_{\rm tele} = 1/[1 + \exp(-2r)]$ for Gaussian states (18). More important for our case, negative features of $W_{\rm in}$ (if any) can only be teleported and retrieved in $W_{\rm out}$ when $F_{\rm tele} \geq 2/3$ (19), a threshold

also known as the no-cloning limit (20). However, the practical lower bound on F_{tele} will be higher because of decoherence and experimental imperfection of W_{in} (21). We have thus defined the success criterion of Schrödinger's-cat-state teleportation as the successful transfer of its nonclassical features, or alternatively, successful teleportation of the Wigner function W_{in} negativity.

Our experimental quantum teleporter and Schrödinger's-cat-state source (Fig. 1) upgrade the experiments described in (3) and (10), respectively. We use three optical parametric oscillators to generate the necessary squeezed vacua. One is used for the Schrödinger's-cat-state preparation; the other two are combined together on a half beam splitter whose two exit ports are the resulting pair of EPR-correlated beams. The teleportation is conducted in three steps. Alice first

receives both the input state and her EPR beam and performs two joint quadrature measurements, obtaining results x_0 and p_0 . Bob then receives Alice's measurements $\beta = (x_0 + ip_0)/\sqrt{2}$ through the classical channels and applies the displacement operator $\hat{D}(\beta)$ on his EPR beam. A final stage consists of a third homodyne detector for tomography at the teleporter output. We emphasize that Alice and Bob do not assume any prior knowledge of the input state and adhere to unity-gain teleportation, so that the teleporter does not have any restriction regarding the specific family of quantum states it can faithfully teleport.

To benchmark our teleporter, we first evaluate the fidelity $F_{\rm tele}$ of teleportation of the vacuum state $|0\rangle$, the coherent state of amplitude zero. At quantum optical frequencies where the mean

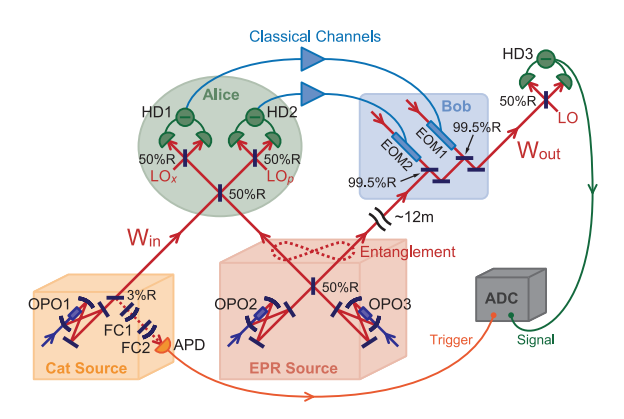


Fig. 1. Experimental setup. OPO, optical parametric oscillator; APD, avalanche photodiode; HD, homodyne detector; LO, local oscillator; EOM, electro-optical modulator; ADC, analog-to-digital converter; FC, filtering cavity. See (12) for details.

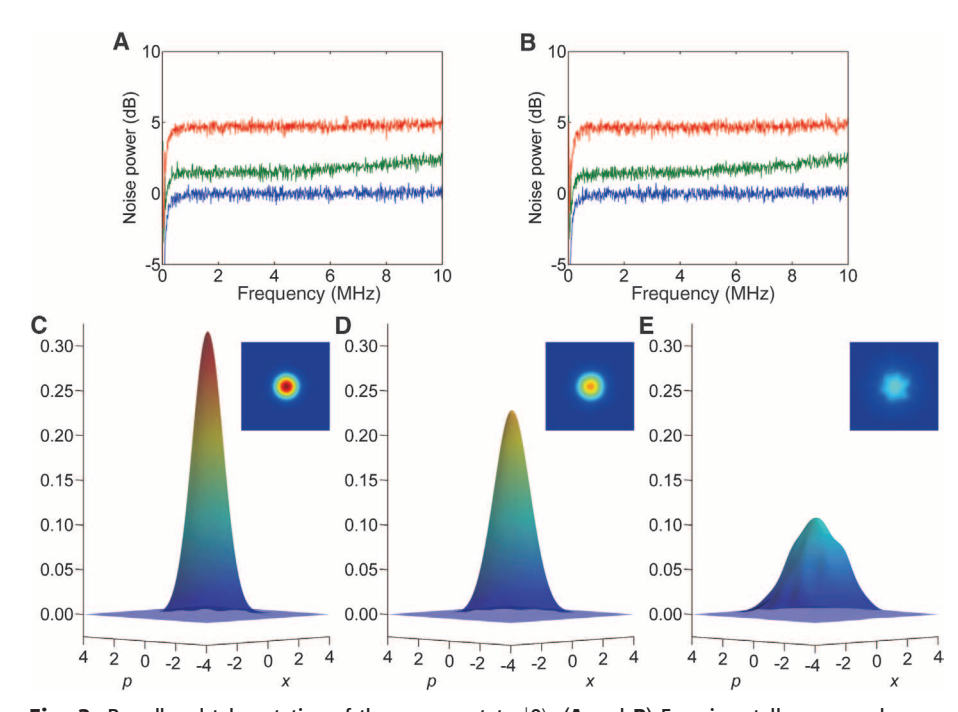


Fig. 2. Broadband teleportation of the vacuum state $|0\rangle$. (**A** and **B**) Experimentally measured power spectra of the photocurrents calculated by Fourier transform are shown for the position (**A**) and momentum (**B**) quadratures. Blue, shot-noise input; green, quantum teleportation output; red, teleportation output without entanglement. (**C** to **E**) Reconstructed Wigner functions of the input state $|0\rangle$ (**C**), quantum teleported vacuum (**D**), and classically teleported vacuum (**E**).

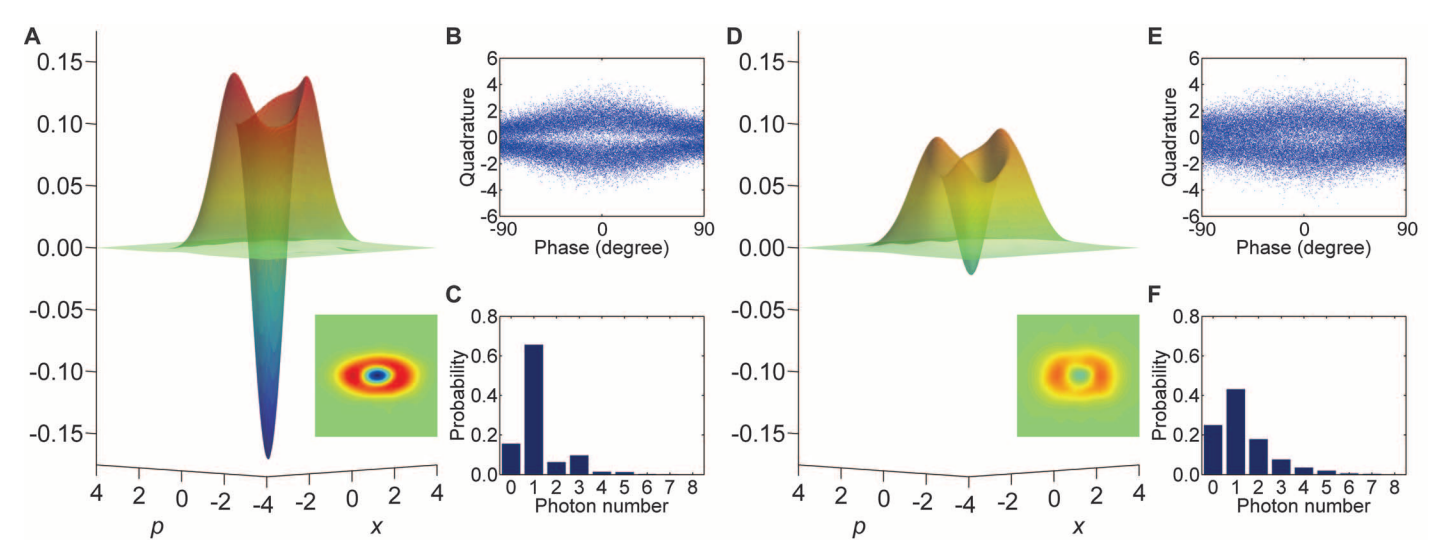


Fig. 3. Teleportation of Schrödinger's-cat states. (A to C) Experimentally measured input state's Wigner function $W_{\rm in}$ (A), marginal distribution (B), and photon number distribution (C). (D to F) Experimentally measured output state's Wigner function $W_{\rm out}$ (D), marginal distribution (E), and photon number distribution (F).

thermal photon number is virtually 0, this is simply done by blocking the input port of the teleporter. The teleported vacuum photocurrent is expected to have uniform Gaussian statistics with a variance $\sigma^2 = \frac{1}{2} + [\exp(-2r)]$ ($\hbar = 1$) from which we can deduce teleportation fidelity (Fig. 2). The blue traces are the shot-noise level, the noise spectrum of the input vacuum $|0\rangle$. The red traces are the classical limit of teleportation obtained by turning off the entanglement between Alice and Bob (r = 0). We measure 4.8 dB of added noise above the shot noise, in agreement with the expected teleportation fidelity of 0.5. When Alice and Bob share entanglement, the added noise drops to that shown by the green traces: 1.4 dB above the shot noise around 1 MHz, corresponding to a fidelity of 0.83. This is in agreement with the experimental figure of -6.9 dB that we observe in direct measurement of the EPR correlations shared between Alice and Bob.

In contrast to quantum teleportation experiments conducted to date for narrow sidebands of light (2, 3), our setup operates over a wide frequency bandwidth, as required by the nature of our input state. Because its generation relies on the detection of a single photon and the induced projection, a Schrödinger's-cat state made via photon subtraction is a short wave packet of light. A phenomenological way to picture these wave packets is to consider them as the closed boxes containing the macroscopic superposition states as in Schrödinger's original idea. This requires Alice and Bob to teleport every frequency component of these "box-like" wave packets for faithful teleportation to occur. In this way, Alice and Bob do not need to actually teleport the Schrödinger's-cat states directly, but merely the potential boxes containing them. Consequently, Alice and Bob do not need to know when a detection event occurs; rather, they are only concerned with continuous and faithful "box" wavepacket teleportation, whichever state lies in the

box. In fact, Alice and Bob actually teleport most of the time a squeezed vacuum state $\hat{S}(s)|0\rangle$.

In essence, our teleporter is a time-resolved apparatus that deconstructs the input wave packets into a stream of infinitely small time bins and reconstructs them at the output, within the extent of what we refer to as the teleportation bandwidth. This bandwidth is clearly visible in both of the green experimental traces where the added noise slowly increases with frequency (Fig. 2). This is a direct consequence of the finite bandwidth of squeezing used for entanglement. However, across the frequencies relevant to our input state, teleportation fidelity is always greater than the no-cloning limit of 2/3, a necessary regime for negativity teleportation. A very careful implementation of the classical channel has been required (12) to achieve experimental realization of this fidelity.

To verify the success of Schrödinger's-catstate teleportation, we perform experimental quantum tomography of the input and output states independently (Fig. 3). Both input and output marginal distributions exhibit the characteristic eye shape of photon-subtracted squeezed states, with a clear lack of detection events around the origin for any phase. Although necessary, this feature alone is not sufficient to confirm the presence of negativity in $W_{\rm in}$ or $W_{\rm out}$. The reconstructed input Wigner function W_{in} shows the two positive Gaussians of $|\alpha\rangle$ and $|-\alpha\rangle$ together with a central negative dip $[W_{in}(0, 0) = -0.171 \pm 0.003]$ caused by the interferences of the $|\alpha\rangle$ and $|-\alpha\rangle$ superposition. The output Wigner function W_{out} retains the characteristic non-Gaussian shape as well as the negative dip $[W_{out}(0, 0) = -0.022 \pm 0.003]$ to a lesser degree. The degradation of the central negative dip and the full evolution of $W_{\rm in}$ toward W_{out} can be fully understood using Eq. 1 with a model of $W_{\rm in}$, as was done in (21). Given the measured input state negativity of $W_{in}(0, 0) = -0.171$ and -6.9 dB of squeezing, the results of (21) predict an output negativity value of -0.02, in good

agreement with measured output negativity. Although this figure does not take into account the input-state squeezing, a more detailed model shows that a squeezing parameter s = 0.28 affects output negativity in the third decimal place only (12). The experimental input and output states have an average photon number $\langle \hat{n} \rangle$ equal to 1.22 \pm 0.01 and 1.33 ± 0.01 , respectively (12). The increase in the output-state size is due to teleportationinduced thermalization. We calculate that the fidelity F_{cat} is as high as 0.750 ± 0.005 for the input Wigner function $W_{\rm in}$, with the nearest Schrödinger'scat state having an amplitude $|\alpha_{in}|^2 = 0.98$ (12). However, after the teleportation W_{out} , fidelity is reduced to 0.46 ± 0.01 , with the nearest Schrödinger'scat state having an amplitude $|\alpha_{\rm out}|^2 = 0.66$. If $W_{\rm out}$ fidelity is calculated with $|\alpha_{\rm in}|^2 = 0.98$, then $F_{\rm cat} = 0.45 \pm 0.01$.

We have demonstrated an experimental quantum teleporter able to teleport full wave packets of light up to a bandwidth of 10 MHz while at the same time preserving the quantum characteristic of strongly nonclassical superposition states, manifested in the negativity of the Wigner function. Although F_{cat} and W(0, 0) drop in the teleportation process, there is no theoretical limitation other than available squeezing, and stronger EPR correlations would achieve better fidelity and negativity transmission. The various more complex states generated as an application of photon subtraction so far (22, 23) can be, in principle, readily sent through our broadband quantum teleporter. This opens the door to universal QIP and further hybridization schemes between discrete- and continuous-variable techniques (24).

References and Notes

- 1. C. H. Bennett *et al.*, *Phys. Rev. Lett.* **70**, 1895
- 2. A. Furusawa et al., Science 282, 706 (1998).
- M. Yukawa, H. Benichi, A. Furusawa, *Phys. Rev. A* 77, 022314 (2008).
- 4.]. Yoshikawa et al., Phys. Rev. A 76, 060301 (2007).

- 5. S. Lloyd, S. L. Braunstein, *Phys. Rev. Lett.* **82**, 1784 (1999).
- M. Dakna, T. Anhut, T. Opatrny, L. Knöll, D.-G. Welsch, *Phys. Rev. A* 55, 3184 (1997).
- A. P. Lund, T. C. Ralph, H. L. Haselgrove, *Phys. Rev. Lett.* 100, 030503 (2008).
- 8. A. Ourjoumtsev, R. Tualle-Brouri, J. Laurat, P. Grangier, *Science* **312**, 83 (2006).
- J. S. Neergaard-Nielsen, B. M. Nielsen, C. Hettich, K. Mølmer, E. S. Polzik, *Phys. Rev. Lett.* 97, 083604 (2006).
- K. Wakui, H. Takahashi, A. Furusawa, M. Sasaki, *Opt. Exp.* 15, 3568 (2007).
- 11. A. Ourjoumtsev, H. Jeong, R. Tualle-Brouri, P. Grangier, Nature 448, 784 (2007).
- 12. See supporting material on Science Online.
- H. Jeong, A. P. Lund, T. C. Ralph, *Phys. Rev. A* 72, 013801 (2005).
- M. Hillery, R. F. O'Connell, M. O. Scully, E. P. Wigner, *Phys. Rep.* **106**, 121 (1984).

- D. T. Smithey, M. Beck, M. G. Raymer, A. Faridani, *Phys. Rev. A* 70, 1244 (1993).
- 16. A. I. Lvovsky, J. Opt. B 54, S556 (2004).
- S. L. Braunstein, H. J. Kimble, *Phys. Rev. Lett.* **80**, 869 (1998).
- 18. B. Schumacher, Phys. Rev. A 54, 2614 (1996).
- 19. M. Ban, Phys. Rev. A 69, 054304 (2004).
- F. Grosshans, P. Grangier, Phys. Rev. A 64, 010301(R) (2001).
- L. Mišta Jr., R. Filip, A. Furusawa, *Phys. Rev. A* 82, 012322 (2010).
- 22. H. Takahashi et al., Phys. Rev. Lett. 101, 233605 (2008).
- J. S. Neergaard-Nielsen et al., Phys. Rev. Lett. 105, 053602 (2010).
- D. Gottesman, A. Kitaev, J. Preskill, *Phys. Rev. A* 64, 012310 (2001).
- 25. Supported by the Strategic Information and Communications R&D Promotion (SCOPE) program

of the Ministry of Internal Affairs and Communications of Japan, Special Coordination Funds for Promoting Science and Technology, Grants-in-Aid for Scientific Research, Global Center of Excellence, Advanced Photon Science Alliance, and Funding Program for World-Leading Innovative R&D on Science and Technology (FIRST) commissioned by the Ministry of Education, Culture, Sports, Science and Technology of Japan, Academy of Sciences of the Czech Republic, Japanese Society for the Promotion of Science, and the Australian Research Council, Center of Excellence (grant CE11E0096).

Supporting Online Material

www.sciencemag.org/cgi/content/full/332/6027/330/DC1 Materials and Methods

30 November 2010; accepted 14 February 2011 10.1126/science.1201034

Enhanced Enantioselectivity in Excitation of Chiral Molecules by Superchiral Light

Yiqiao Tang¹ and Adam E. Cohen^{1,2}*

A molecule or larger body is chiral if it cannot be superimposed on its mirror image (enantiomer). Electromagnetic fields may be chiral, too, with circularly polarized light (CPL) as the paradigmatic example. A recently introduced measure of the local degree of chiral dissymmetry in electromagnetic fields suggested the existence of optical modes more selective than circularly polarized plane waves in preferentially exciting single enantiomers in certain regions of space. By probing induced fluorescence intensity, we demonstrated experimentally an 11-fold enhancement over CPL in discrimination of the enantiomers of a biperylene derivative by precisely sculpted electromagnetic fields. This result, which agrees to within 15% with theoretical predictions, establishes that optical chirality is a fundamental and tunable property of light, with possible applications ranging from plasmonic sensors to absolute asymmetric synthesis.

ircular dichroism (CD) describes the differential absorption of left- and right-circularly polarized light by a chiral molecule (1). CD spectroscopy provides important structural information and is widely used for characterizing organic and biological molecules. Yet CD measurements are challenging because the signals are typically weak. For most small molecules, the absorption cross sections for left-and right-circularly polarized light differ by less than one part per thousand (2).

The weakness of CD is a consequence of the small size of most molecules relative to the wavelength of light: The circularly polarized field undergoes a barely perceptible twist over a distance of molecular dimensions (3). This twist provides only a weak perturbation to the overall rate of excitation. Finding ways to enhance CD could lead to improved sensors and may open the door to efficient absolute asymmetric synthesis in which light provides the chiral bias.

Substantial effort has been devoted to calculating CD spectra for a variety of molecules at multiple levels of theory (4, 5) and to designing molecules that show large optical dissymmetry at particular wavelengths (2). These treatments focused on the molecular aspects of CD, relying on circularly polarized plane waves as the source of excitation.

With the advent of near-field optics, plasmonics, photonic crystals, and metamaterials, scientists now construct electromagnetic fields that are far more contorted than is circularly polarized light (CPL) (6, 7). Several groups have sought to use metallic nanostructures to enhance chiroptical phenomena (8-10). Recently, Hendry et al. reported enhanced CD in samples of proteins adsorbed onto chiral metal nanostructures (11). These experiments may lead to important practical applications, but the complexity of the geometries has thus far prevented a quantitative comparison with theory. Other groups have applied techniques of coherent control to enantioselective excitation of chiral molecules, but these strategies are specific to a single compound or narrow class of compounds (12).

We wondered whether it would be possible to design non-plane-wave monochromatic solutions to Maxwell's equations that showed enhanced dissymmetry in their excitation of all chiral molecules, regardless of molecular structure. Our intuitive picture was that enhanced dissymmetry should occur if the field lines reoriented over a distance much shorter than the free-space wavelength, ideally over molecular dimensions. Then the spatial scales of chirality in the molecule and the light would match (13).

To guide the design of superchiral light, we sought a measure of optical chirality, a way to determine whether one field couples more strongly to molecular chirality than does another (14). Such a measure must have certain symmetries. Chirality is time even (a movie of a right-handed screw shows a right-handed screw whether the movie is played forward or backward), parity odd (a mirror image of a right-handed screw is a lefthanded screw), and scalar (a right-handed screw remains right-handed no matter its orientation). A classification of the well-known conserved electrodynamic quantities by their symmetries (Fig. 1A) reveals a vacancy where there should be a timeeven, parity-odd scalar. Any measure of optical chirality must lie in this empty fourth quadrant (15).

On the basis of these symmetry considerations, we proposed the existence of a physical quantity, optical chirality, defined in Fig. 1A. The mathematical structure of optical chirality captures the degree to which the electric and magnetic field vectors **E** and **B** wrap around a helical axis at each point in space. In the 1960s, Lipkin studied this same quantity, but he and others dismissed it as lacking physical significance (16, 17).

Is optical chirality observable? In the standard theory of CD, the dissymmetry factor, $g(\lambda)$, measures the fractional difference in rates of excitation between left- and right-circularly polarized light at wavelength λ (18). We generalized the theory of CD to include pairs of arbitrary mirror-image fields and found that the dissymmetry factor becomes (14)

$$g = g_{\text{CPL}} \left(\frac{cC}{2U_{\text{e}}\omega} \right) \tag{1}$$

where g_{CPL} is the dissymmetry factor under circularly polarized light, c is the speed of light,

¹Department of Physics, Harvard University, 12 Oxford Street, Cambridge, MA 02138, USA. ²Department of Chemistry and Chemical Biology, Harvard University, 12 Oxford Street, Cambridge, MA 02138, USA.

^{*}To whom correspondence should be addressed. E-mail: cohen@chemistry.harvard.edu